The EMBO Journal vol.13 no.6 pp.1255–1262, 1994

Three-dimensional structure of 6-pyruvoyl tetrahydropterin synthase, an enzyme involved in tetrahydrobiopterin biosynthesis

Herbert Nar, Robert Huber, Claus W.Heizmann[1], Beat Thöny[1] and Daniel Bürgisser[1]

Max Planck Institut für Biochemie, Abteilung Strukturforschung, Am Klopferspitz, D-82152 Martinsried, Germany and [1]Division of Clinical Chemistry, Department of Pediatrics, Universität Zürich, CH-8032 Zürich, Switzerland

Communicated by R.Huber

The crystal structure of rat liver 6-pyruvoyl tetrahydropterin synthase has been solved by multiple isomorphous replacement and refined to a crystallographic *R*-factor of 20.4% at 2.3 Å resolution. 6-Pyruvoyl tetrahydrobiopterin synthase catalyses the conversion of dihydroneopterin triphosphate to 6-pyruvoyl tetrahydropterin, the second of three enzymatic steps in the synthesis of tetrahydrobiopterin from GTP. The functional enzyme is a hexamer of identical subunits. The 6-pyruvoyl tetrahydropterin synthase monomer folds into a sequential, four-stranded, antiparallel β-sheet with a 25 residue, helix-containing insertion between strands 1 and 2 at the bottom of the molecule, and a segment between strands 2 and 3 forming a pair of antiparallel helices, layered on one side of the β-sheet. Three 6-pyruvoyl tetrahydropterin synthase monomers form an unusual 12-stranded antiparallel β-barrel by tight association between the N- and C-terminal β-strands of two adjacent subunits. The barrel encloses a highly basic pore of 6–12 Å diameter. Two trimers associate in a head-to-head fashion to form the active enzyme complex. The substrate-binding site is located close to the trimer–trimer interface and comprises residues from three monomers: A, A′ and B. A metal-binding site in the substrate-binding pocket is formed by the three histidine residues 23, 48 and 50 from one 6-pyruvoyl tetrahydropterin synthase subunit. Close to the metal, but apparently not liganding it, are residues Cys42, Glu133 (both from A) and His89 (from B), which might serve as proton donors and acceptors during catalysis.

Key words: biosynthesis/crystal structure/hyperphenylalaninaemia/6-pyruvoyl tetrahydropterin synthase/tetrahydrobiopterin

Introduction

6*R*-L-Erythro-5,6,7,8-tetrahydrobiopterin (BH_4) is the natural co-factor for several important enzymes, such as the aromatic amino acid hydroxylases (Nichol *et al.*, 1985), nitric oxide synthase (Kwon *et al.*, 1989; Tayeh and Marletta, 1989) and glycerol ether monooxygenase (Kaufman *et al.*, 1990). Lack of the co-factor in man leads to a malfunction of phenylalanine catabolism and a deficiency of the biogenic amine neurotransmitters, dopamine and serotonin (Scriver *et al.*, 1989). Clinical symptoms of this so-called hyperphenylalaninaemia due to BH_4 deficiency are severe neurological disorders and mental retardation (Kaufman *et al.*, 1978; Niederwieser *et al.*, 1984; Blau, 1988). The most common form of BH_4 deficiency is due to the autosomal recessively inherited absence of 6-pyruvoyl tetrahydropterin synthase (PTPS) activity (Blau *et al.*, 1993).

PTPS (EC 4.6.1.10) catalyses the second reaction in the three-step biosynthesis of BH_4 from GTP (Figure 1A; Curtius *et al.*, 1985). The reaction involves a complex remodelling of the substrate, dihydroneopterin triphosphate, via a base-catalysed, internal redox transfer and triphosphate elimination (Figure 1B; Le Van *et al.*, 1988).

PTPS has been isolated from human (Takikawa *et al.*, 1986), rat (Inoue *et al.*, 1991) and salmon liver (Hasler and Curtius, 1989; Hauer *et al.*, 1992), human pituitary gland (Guzman *et al.*, 1992), *Drosophila melanogaster* (Park *et al.*, 1990) and silkworm larvae (Masada, 1993). Recently, the cDNA encoding this enzyme in rat and human liver has been cloned and expressed in *Escherichia coli* (Inoue *et al.*, 1991; Thöny *et al.*, 1992). The cDNAs encode amino acid sequences of 144 (rat) and 145 (human) residues. Comparison with the sequence of native rat liver PTPS indicates that the 'mature' protein lacks the four N-terminal amino acid residues (Inoue *et al.*, 1991). The native N-terminus of the human liver enzyme is not known.

Recombinant expression of the rat and human PTPS has allowed the investigation of some of the biochemical properties of the enzyme (Bürgisser *et al.*, 1994). Cross-linking experiments have shown that the enzyme in solution exists as a homohexamer which is dissociable into trimers. The free thiol group of the conserved residue Cys42 in the rat sequence (Cys43 in the human sequence) and the presence of divalent cations such as Mg^{2+} have been implicated in its activity.

Here, we present the three-dimensional structure of rat liver PTPS, the first enzyme of the BH_4 biosynthetic pathway to be structurally characterized. The 82% sequence identity to the human liver PTPS ensures that conclusions based on the present structure will apply to the human enzyme as well. In particular, it will be possible to analyse the structural basis for BH_4 deficiency in hyperphenylalaninaemic patients.

Results

Secondary and tertiary structure

The crystal structure of the 'mature' (Inoue *et al.*, 1991) form of rat liver PTPS (residues 5–144 encoded by the cDNA) was solved by multiple isomorphous replacement. The crystallographic model comprises residues 7–144 which fold into a compact, single-domain α + β structure (Levitt and Chothia, 1976). A sequential, four-stranded, antiparallel β-sheet is composed of residues 8–24, 48–60, 128–133 and 137–142. Layered onto one side of this β-sheet are two

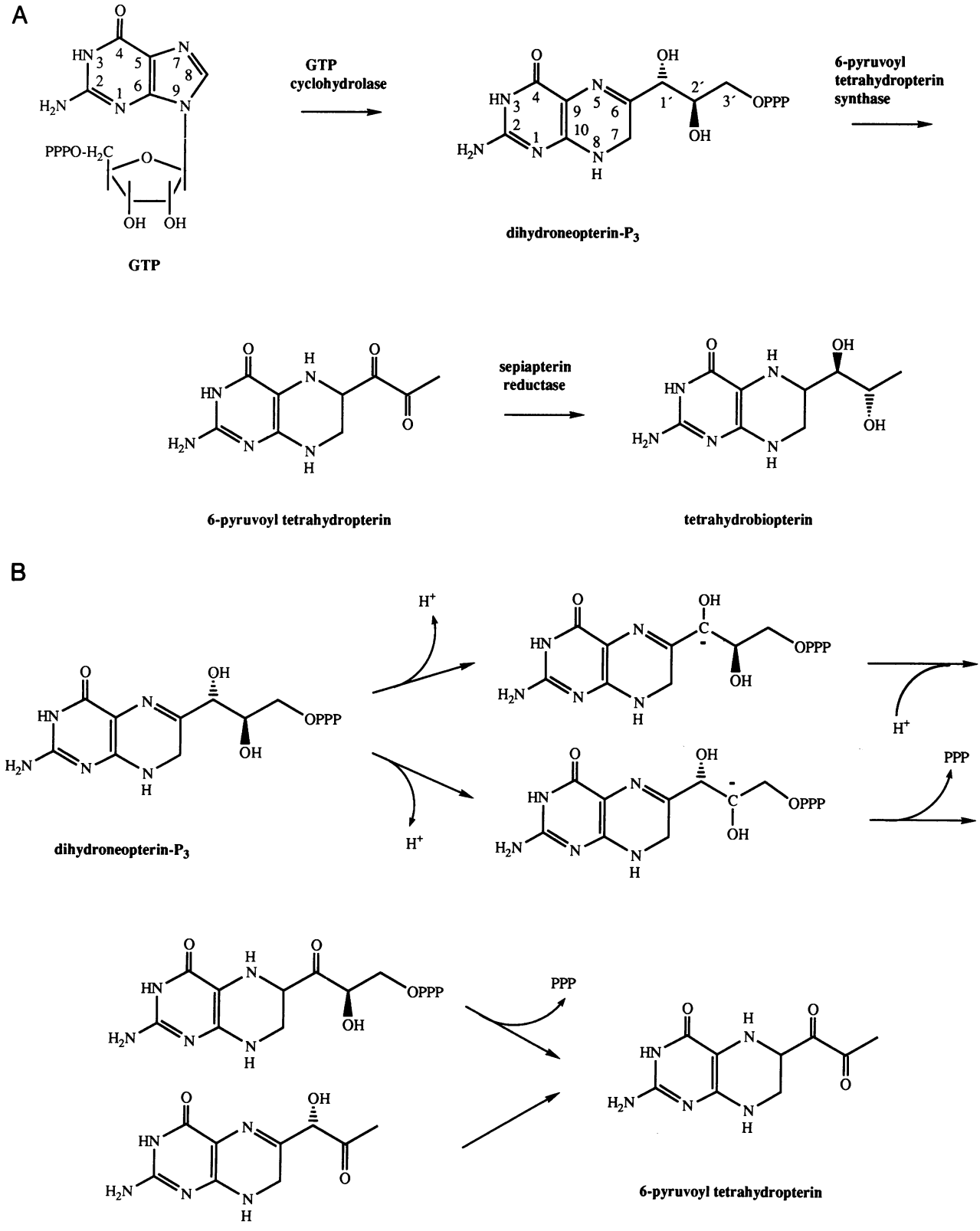

Fig. 1. (**A**) Three-step biosynthetic pathway from GTP to tetrahydrobiopterin. The intermediates, dihydroneopterin triphosphate and 6-pyruvoyl tetrahydropterin, are unstable. (**B**) Hypothetical reaction mechanism of 6-pyruvoyl tetrahydropterin synthase (Le Van *et al.*, 1988). Two alternative reaction paths are proposed. Triphosphate elimination may occur upon proton abstraction from C-2′, followed by a tautomerization step and formation of a methylketone intermediate. The latter is converted to 6-pyruvoyl tetrahydropterin via a base-catalysed (proton abstraction from C-1′) redox transfer involving atoms N-5, C-6 and C-1′. In the alternative pathway, the order of the steps is reversed, i.e. the redox transfer takes place prior to triphosphate elimination. Labelling studies have demonstrated that the protons in the product on N-5, C-6 and C-3′ originate from the solvent (Smith and Nichol, 1983; Curtius *et al.*, 1985; Kerler *et al.*, 1989), suggesting that the catalytic bases are accessible to solvent and exchange their protons rapidly.

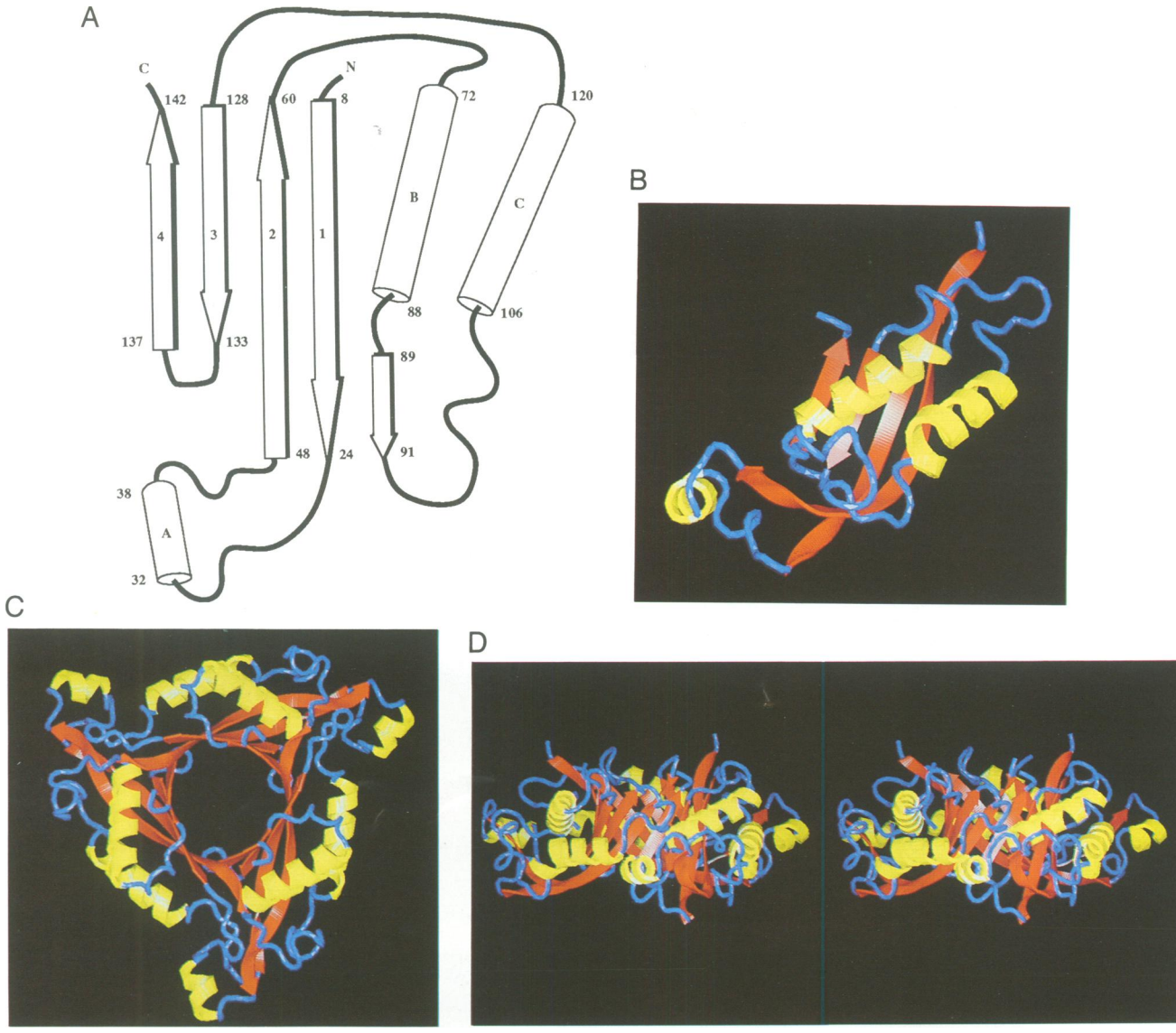

Fig. 2. (**A**) Schematic representation of the secondary structural elements of a 6-pyruvoyl tetrahydropterin synthase monomer with the numbering of the β-strands and α-helices. (**B**) Fold of the monomer of 6-pyruvoyl tetrahydropterin synthase drawn in a ribbon-type representation. Red arrows represent β-strands, the yellow spirals α-helical regions and the blue lines connecting loops lacking extended secondary structure elements. The antiparallel β-sheet is formed by sequential alignment of β-strands, i.e. strand 1 is furthest to the right and is hydrogen bonded to strand 2, the latter one to strand 3 which is in contact with strand 4 (left-most arrow). The two-turn helix A within the 25 residue insert between strands 1 and 2 (helix appendix) forms the bottom of the molecule. Two antiparallel helices (B and C) in a sequence segment between strands 2 and 3 are layered on the top face of the sheet. (**C**) 6-Pyruvoyl tetrahydropterin synthase trimer viewed along the three-fold symmetry axis. The three 4-stranded β-sheets of all subunits assemble to a 12-stranded antiparallel β-barrel, which is surrounded by a layer of helices. The trimer is disc shaped with a diameter of 60 Å. (**D**) Stereo view of the trimer viewed perpendicular to the trimer axis showing the perfection of the β-barrel construction. The chain termini are all located on the upper face of the trimer disc.

antiparallel α-helices comprising residues 72−88 and 106−120 in a sequence segment inserted between β-strands 2 and 3. The helices are connected through a polypeptide stretch folded into a sequence of helical turns and a short tripeptide (89−91) which adopts a β-strand conformation and extends the β-sheet structure by hydrogen bonding to residues 20−24 of β-strand 1. Between strands 1 and 2, there is a 25 residue insert containing a two-turn α-helix (residues 32−38) which lies below the two longer helices on the same face of the β-sheet. Strands 3 and 4 are connected via an α-helical turn made by residues 134−136 (Figure 2A and B).

The domain has an ellipsoidal shape with dimensions 60 × 25 × 18 Å. Its topology belongs to a family of structures characterized by a packing of a layer of β-sheet against a layer of α-helices, both enclosing a hydrophobic core (Orengo and Thornton, 1993). The secondary structure sequence βαβααββ in the described three-dimensional arrangement, however, represents a novel protein fold to the best of our knowledge.

Trimer and hexamer assembly

In the crystal structure, three monomers of PTPS related by the crystallographic 3-fold symmetry axis assemble into a trimer by tight hydrogen bonding between the N- and C-terminal β-strands of adjacent monomers. A 12-stranded

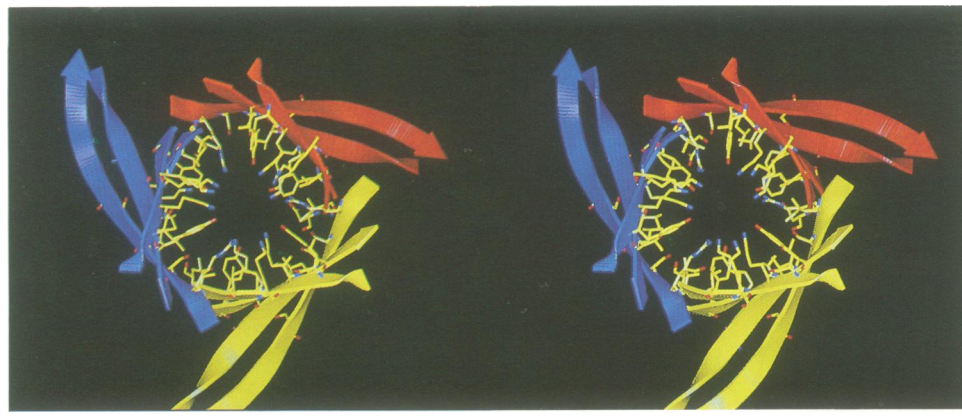

Fig. 3. Stereo view of the trimer channel. The β-sheet structure of the trimer resembles the appearance of propeller blades. The interior of the pore is formed by the side chains of Arg12, Lys53, Lys128, Lys130 and Lys142, as well as Tyr127 and Tyr132 from each subunit which stretch radially into the pore. Other residues contributing to the channel wall are either hydrophobic or uncharged polar (residues Ser14, Leu16, Ser18, Val55, Thr57, Ile138 and Val140). The diameter of the pore is 6 Å at the upper end where the chain termini are located and enlarges to 12 Å at the bottom due to the conical shape of the barrel.

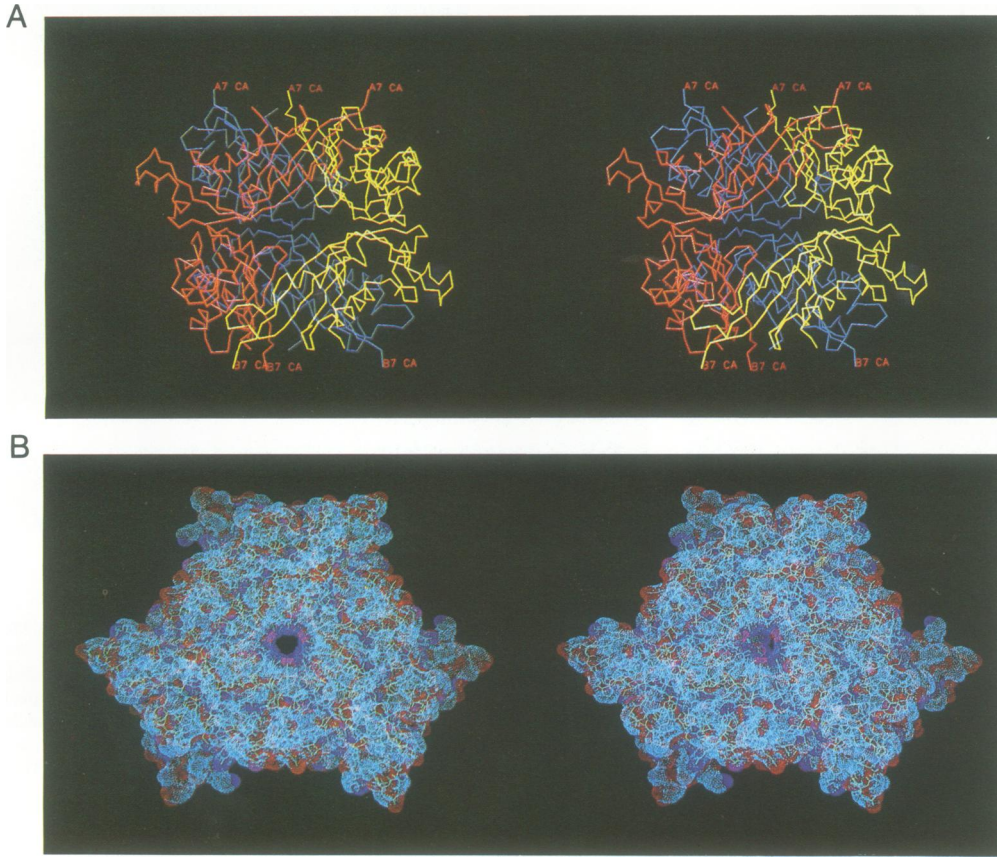

Fig. 4. (**A**) Stereo picture of a Cα trace of the 6-pyruvoyl tetrahydropterin synthase hexamer. The hexamer is a trimer of dimers. A tight contact exists within the dimer by the stacking of two dyad related β-sheet regions whose strands run perpendicular to each other. The hexamer encapsulates a large cavity which can be accessed via the basic pores along the trimer axis, as well as through large openings on the hexamer equator.
(**B**) Connolly surface of the hexamer (colour code: light blue, carbon atoms; dark blue, nitrogen atoms; red, oxygen atoms; yellow, sulphur atoms) viewed along the three-fold axis. There are no surface regions which exhibit a particular charge pattern, except for the channel walls, which are highly positively charged, as visualized by the dark blue colour at the pore entrance.

antiparallel β-barrel structure is thereby formed, surrounded by a ring of α-helices (Figure 2C and D). The trimer is disc shaped with 60 Å diameter and a height of 30 Å.

The monomers are held together not only by perfect antiparallel β-strand interactions between residues 11–15 on the N-terminal and residues 136–141 on the C-terminal strands, but are interlocked via additional interactions between the loop regions 62–72 on one and 102–111 on the neighbouring subunit. The β-strands of the barrel are tilted by 30° with respect to the crystallographic triad. The barrel is conically shaped with the smaller opening on the side where the monomer chain termini are located. It

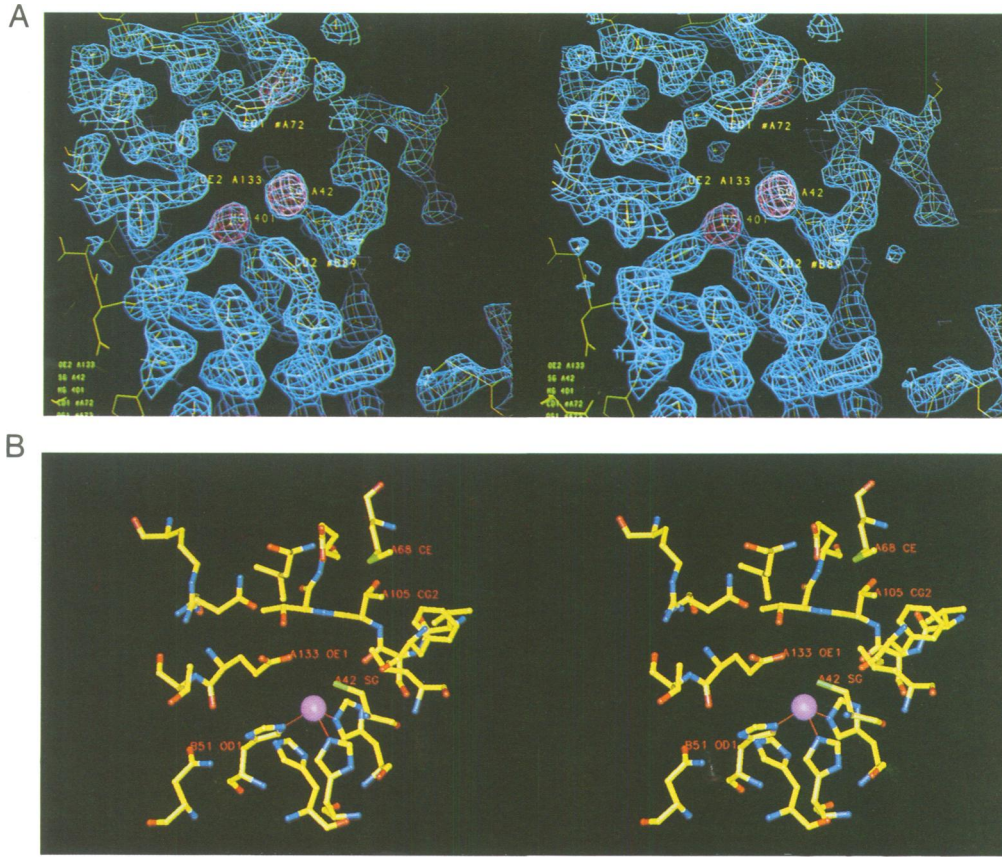

Fig. 5. (**A**) $2F_o-F_c$ electron density (light blue) around the metal-binding site contoured at 1.4σ and superimposed on the refined model of 6-pyruvoyl tetrahydropterin synthase. F_o-F_c omit map electron density (red) contoured at 5σ. This map was calculated with phases lacking the structure factor contribution of the metal ion and the sulphur atoms of Cys42 and Met68. (**B**) Atomic structure of the putative substrate-binding site of 6-pyruvoyl tetrahydropterin synthase. The metal ion is represented by the sphere (magenta). The ion is bound to three histidine residues from one 6-pyruvoyl-tetrahydropterin synthase subunit (His23, His48 and His50) at 2.3 Å distance. Three residues, Cys42, Glu133 from the same subunit and His89 from the neighbouring monomer, are positioned very close to the metal-binding site and might serve as proton donors and acceptors during catalysis.

encloses a hydrophilic pore of 6–12 Å diameter. An unusual cluster of basic and aromatic residues accumulates in the barrel interior. Four lysines, one arginine and two tyrosine residues from each subunit stretch radially into the pore, whose wall is complemented by eight additional hydrophobic or uncharged polar side chains (Figure 3).

At physiological pH (as well as at the pH of crystallization), and assuming normal pK_as of arginines and lysines, the basic residues are protonated. There are residual electron density peaks which have been interpreted as solvent molecules. However, they may represent OH^-, Cl^- or SO_4^{2-} anions acting as counter ions.

An almost perfect local 2-fold symmetry axis perpendicular to the crystallographic triad relates two trimers which arrange in a head-to-head fashion to form a PTPS hexamer (Figure 4A and B). The contact region between PTPS trimers is formed by the 'horizontal' part of the β-sheet of two monomers (residues 20–24, 48–51 and 89–91). The β-strands of the two subunits are <4 Å apart and run almost perpendicular to each other. The hexamer arrangement is stabilized by heterologous, rotationally symmetrical hydrogen bonds between subunits A and B (Asn B51 Nδ-H ... O His A50, Asn B51 Oδ ... H-Nδ His A50, Thr B20 Oγ-H ... O Gly A49).

The hexameric nature of PTPS was unanticipated prior to determination of its three-dimensional structure. Although a tendency of monomers to oligomerize was known, the existence of a defined oligomer was obscured by the determination of variable apparent molecular weights by gel-filtration experiments (Takikawa *et al.*, 1986; Hasler and Curtius, 1989; Inoue *et al.*, 1991; Guzman *et al.*, 1992). During the course of the crystallographic work, we performed cross-linking studies and demonstrated that the predominant form of human PTPS in solution is hexameric (Bürgisser *et al.*, 1994), in line with the results obtained here. The overall dimensions of the PTPS hexamer are ~60 × 60 × 60 Å. As a consequence of the conical shape of the β-barrel of both trimers, the hexamer encloses a large solvent-filled cavity of dimensions 20 × 20 × 15 Å which opens up not only to the barrel pores, but also equatorially to the hexamer surroundings (Figure 4A).

Active site structure

Alkylating sulfhydryl reagents inactivate the enzymes from silkworm (Masada, 1993) and human and rat liver (Bürgisser *et al.*, 1993). The conserved residue Cys42 (rat sequence) protrudes from the connecting α-helical turn between helix A and β-strand 2 into a cleft formed by the lower part of the β-sheet and the N-terminal end of helix C.

In close proximity to the Cys42 thiol group, three histidine side chains from residues His23, His48 and His50 point upwards from the β-sheet scaffold, forming the floor of the

Table I. Qualitative assessment of the enzyme activity as a function of the nature of the activating metal ion

Metal ion (5 mM)	apo	Ca^{2+}	Cu^{2+}	Zn^{2+}	Mn^{2+}	Fe^{2+}	Co^{2+}	Ni^{2+}	Mg^{2+}
Enzyme activity									
Rat PTPS	–	–	–	–	+	+	+	++	+++
Human PTPS	–	–	–	–	+	++	+	++	+++

A total of 100 μg human or rat PTPS were treated with 50 mM EDTA and EGTA and 5 mM *o*-phenanthroline in 500 μl 50 mM Tris. For the activity measurements, 1 μU enzyme was used.

cleft. To our surprise, a large residual peak showed up in the $2F_o-F_c$ electron density in this area that fuses the densities of the imidazole rings of the histidines (Figure 5A). From omit maps, this peak was estimated as ~20 electrons. Therefore, we have interpreted it as a metal atom bound to the histidines.

It had been shown previously that PTPS activity depends on the presence of Mg^{2+} which is also used in the standard activity assay (Takikawa *et al.*, 1986). Some reports have indicated that other metals, like Ca^{2+}, Ba^{2+} and Mn^{2+}, can substitute for Mg^{2+} (Inoue *et al.*, 1991; Masada, 1993); however, results were ambiguous. The particular co-ordination environment of three histidine side chains liganding with their Nε-atoms is not typical for Mg^{2+}, but is well known from protein and model structures for transition metals such as Zn^{2+}, Cu^{2+}, Mn^{2+} or $Fe^{2+/3+}$ (da Silva and Williams, 1991). We therefore tested enzyme activity as a function of the nature of the metal present in the assay (Table I). The results indicated that indeed Mn^{2+}, $Fe^{2+/3+}$, Co^{2+} and Ni^{2+} partially activate the enzyme, whereas Ca^{2+}, Zn^{2+} and Cu^{2+} are inactive. However, the highest activity was obtained with Mg^{2+}.

The nature of the metal present in PTPS crystals remains obscure, since during isolation and crystallization no metal ions were added intentionally. Incorporation of metal must, therefore, have occurred during cell growth or during crystallization due to metal contamination of the reagents. Refinement of the metal atom occupancy using atomic scattering factors of Mg^{2+} (10 electrons) was consistent with ~20 electrons, suggesting the presence of a transition metal ion rather than a magnesium ion. Identification of the native metal ion requires further experimental confirmation, however.

Crystalline apo-PTPS can be prepared by soaking native crystals in *o*-phenanthroline and EDTA (data not shown). Furthermore, the metal ion is apparently exchangeable by some of the heavy metal ions used for multiple isomorphous replacement, namely Hg^{2+}, Pt^{2+} and Au^{3+}, as shown by difference Fourier syntheses with derivative data sets.

In the refined structure, the metal is co-ordinated by three His Nε at 2.3 Å distance which would occupy the corners of an octahedron around the metal (Figure 5B). The electron density gives no indication, however, of the presence of ligands occupying further sites. The Cys42 sulfur atom, as well as the carboxylate group of Glu133, are close to the metal at 4.5 and 3.8 Å distance, but apparently do not ligand it. Between them, there is space for a fourth ligand which could be a water molecule or bound substrate.

The putative substrate-binding site (Figure 5B) is formed by three PTPS monomers: two from one trimer (A and A′) and one from the other trimer (B). On oligomerization, the cleft containing Cys42 and the metal site on subunit A is closed by two loops on subunit A′ to form a 10 Å deep cavity, the entrance of which is formed by residues from subunit B.

There are six active sites per hexamer. They are located in the vicinity of the equatorial entrances to the solvent-filled centre inside the hexamer shell. The distance from one metal site on monomer A to the one on monomer B is 16 Å. Although the active site pockets are spatially separated, they are interconnected by hydrogen bonds of the Asn51 carbamide moiety to His50 Nδ-H and O on the other subunit.

Discussion

While antiparallel β-barrels are a common protein topology, barrel formation by a three-fold symmetric arrangement of subunits represents a novel structural motif. A similar 12-stranded antiparallel β-barrel has recently been discovered for the cell cycle regulatory protein CksHs2 (Parge *et al.*, 1993). In the latter case, oligomer formation is metal induced and reversible. In contrast, the PTPS hexamer is very probably the functionally active and exclusive form of the enzyme in solution. Since this type of quaternary structure has now been established for two proteins of diverse function, these proteins may represent a new structural family.

The PTPS trimer is reminiscent of porin (Weiss *et al.*, 1991), an integral membrane protein which forms a 16-stranded barrel from one polypeptide chain enclosing a hydrophilic core. The functions of the pores might be similar for the two proteins. In porin, the tunnel serves as a channel through the membrane. The pore in PTPS may also act as a channel for the substrate, dihydroneopterin triphosphate. This compound harbours the negatively charged triphosphate moiety and might therefore enter the tunnel by attractive electrostatic forces of the basic residues. Dihydroneopterin triphosphate is an instable intermediate whose half-life in buffer solution is only very short (Milstien and Kaufman, 1985). Its decomposition involves oxidation of the pterin moiety or triphosphate hydrolysis. An interaction with the protein coat inside the pore could serve to stabilize the substrate and shield it from the solute. Alternatively, the positively charged tunnel wall might stabilize the protonated form of the pterin group of the substrate which is more resistant toward oxidation.

Dihydroneopterin triphosphate is synthesized from GTP by GTP cyclohydrolase I (EC 3.5.4.16), a protein complex consisting of 10 identical subunits arranged as a sandwich of two pentamers with 5_2 symmetry (Schmid *et al.*, 1993). Although the atomic structure of GTP cyclohydrolase is unknown, it is tempting to assume a cylindrical structure of the decamer, perhaps surrounding a similar type of pore. Electron micrographs of freeze-etched cyclohydrolase crystal faces support this notion (Schmid *et al.*, 1993). Complex formation of the GTP cyclohydrolase I decamer with the

Table II. Data collection statistics

Derivative	No. of measurements	Unique reflections	Resolution	Completeness overall/last shell (%/%)	R_m	R_f	Number of sites	Phasing power (20.0–3.0 Å)
NATI 1	73 378	17 425	2.6		12.3	4.0		
NATI 2	97 258	21 645	2.3		11.6	3.6		
NATI 1 + 2		22 612	2.3	92.0/90.7		6.3		
HGAC	127 465	22 096	2.3	91.8/89.7	12.5	3.9	2	1.34
AUCL	40 937	10 127	3.0	92.2/92.3	11.4	4.7	3	1.02
PTCL	34 815	9 947	3.0	90.2/89.4	15.8	5.6	6	0.88
REOX	47 536	10 256	3.0	93.5/94.0	12.3	4.2	6	0.96
YBSO	61 049	10 388	3.0	93.8/92.7	16.1	4.2	3	0.34
MERC	36 947	9 911	3.0	89.9/91.4	13.7	6.2	4	0.89

Overall figure of merit (20.0–3.0 Å) = 0.52.
Derivative soaking conditions: HGAC: Hg(II) acetate 5 mM, 2 days; AUCL: $KAuCl_3$ 10 mM, 5 days; PTCL: K_2PtCl_4 2 mM, 2 days; REOX: (NH_4) ReO_4, 2 mM, 3 days; YBSO: $Yb_2(SO_4)_3$, 15 mM, 4 days; MERC: mercurochrome, 10 mM, 2 days.
$R_M = \Sigma|I_h - <I_h>|/\Sigma <I_h>$; R_F:R_M after independent averaging of Friedel pairs.
Phasing power: $<F_H>/E$, where $<F_H> = \Sigma (f_h^2/n)^{1/2}$ is the r.m.s. heavy atom structure factor amplitude.
$E = \Sigma[(F_{PHC} - F_{PH})^2/n]^{1/2}$ is the residual lack of closure error with F_{PH} being the structure factor amplitude and $F_{PHC} = |\mathbf{F}_P + \mathbf{f}_H|$ the calculated structure factor amplitude of the derivative.

PTPS hexamer could bring both pores on top of each other, in turn facilitating delivery of dihydroneopterin triphosphate to PTPS.

PTPS catalyses the formation of 6-pyruvoyl tetrahydropterin, another instable intermediate in BH_4 biosynthesis which is subsequently reduced by sepiapterin reductase (Figure 1A). The sequence of reactions performing the conversion of dihydroneopterin triphosphate to 6-pyruvoyl tetrahydropterin—internal redox transfer involving N-5, C-6 and C-1′, or triphosphate elimination at the C-2′–C-3′ bond—is not known. Both possible pathways (Figure 1B), however, involve the formation of carbanion intermediates by proton abstraction from either C-1′ and C-2′ of dihydroneopterin triphosphate in each of the two steps (Le Van *et al.*, 1988). Although the individual functional groups undergo oxidation (side chain alcohol groups on C-1′ and C-2′ to keto groups) or reduction (pterin ring from the dihydro- to the tetrahydro-state, C-3′ from alcohol to methyl) there is no net oxidation or reduction of the substrate.

The co-ordination environment found in the crystal structure strongly suggests the binding of a transition metal ion in the active site pocket of the enzyme. The results of the activity tests with different metal ions, however, show that Mg^{2+} is able to activate the enzyme most efficiently. Therefore, the role of the metal ion probably does not involve a redox function. Instead, the metal may serve as a substrate anchor either via interaction with the triphosphate group on the substrate [as suggested for instance for iron in phosphatases (Doi *et al.* (1988)] or with the carbanion intermediates.

The amino acid side chains of Cys42, Glu133 and His89 are possible candidates for being the bases necessary for deprotonation and protonation of the substrate or intermediates during the catalytic cycle.

These residues, as well as others which are mutated in hyperphenylalaninaemic patients (B.Thöny *et al.*, 1994) will be subject to forthcoming site-directed mutagenesis studies in order to elucidate (i) the detailed mechanism of PTPS enzyme catalysis and (ii) the molecular cause of the disease on the basis of the PTPS structure.

Materials and methods

Recombinant rat liver PTPS was prepared as described previously (Bürgisser *et al.*, 1994). Briefly, PTPS was expressed as a fusion protein with maltose-binding protein (MBP) in a transformed *E.coli* TB1 strain. After cell harvesting and lysis, the crude extract was applied to an amylose resin affinity column. The eluted fusion protein was cleaved with Factor Xa. PTPS was separated from MBP by gel filtration, concentrated and stored in 20 mM Tris–HCl buffer (pH 7.5) at 4°C.

Enzyme activity assays were carried out as decribed previously (Takikawa *et al.*, 1986). Apo-PTPS was prepared by dialysis against a mixture of 20 mM *o*-phenanthroline and 50 mM EDTA in buffer solution. The activity tests with different metal ions were performed with apo-PTPS and 5 mM Me^{2+} in the assay mixture (Table I).

Crystallization experiments were performed at 4°C employing the vapour diffusion technique. Hanging droplets were made by mixing 5 μl protein solution [4 mg/ml in 1 mM MES/NaOH (pH 7.5)] and 1.7 μl precipitating buffer. The enzyme was crystallized against 1.3 M ammonium sulfate, 0.1 M Tris–HCl (pH 9.0). Crystals appeared after 10 days and grew to full size within 4 weeks. The crystals are trigonal prisms and belong to space group P321. The lattice constants are a = b = 122.3 Å, c = 61.6 Å, γ = 120°. The asymmetric unit contains two PTPS molecules. The crystals have an unusually high solvent content of 70% (V_m = 4.2 Å^3/Da), but are well ordered and diffract to at least 2.3 Å.

All data were collected on a MAR Research imaging plate detector with graphite-monochromatized Cu-Kα radiation from a Rigaku RU200 rotating anode generator. The generator was operated at 5.4 kW with an apparent focal spot size of 0.3 × 0.3 mm^2.

Data were recorded in frames of 1.0° by rotating the crystal about its c-axis by 60°. Images were processed with MOSFLM (version 4.2, A.G.W.Leslie, unpublished) and data were scaled and reduced using ROTAVATA/AGROVATA of the CCP4 package. Other crystallographic computing was done using the PROTEIN program package (Steigemann, 1974), refinement was carried out with XPLOR (Brünger, 1988) and model building was performed with FRODO (Jones, 1978).

The structure of PTPS was solved by a combination of multiple isomorphous replacement (MIR) and averaging techniques.

Heavy atom derivatives were prepared by soaking crystals in a harvesting buffer [2.5 M ammonium sulfate, 0.1 M Tris–HCl (pH 9.0)] under conditions summarized in Table II. Heavy atom sites were located from isomorphous difference Patterson functions and confirmed by cross-difference Fourier syntheses. Six heavy atom derivatives were used for phase calculation (Table II), which gave an overall figure of merit of 0.52 (20–3.0 Å). The correct hand of a consistent set of heavy atom sites of the three derivatives HGAC, AUCL and PTCL was determined by solvent flattening and phase combination after inclusion of anomalous dispersion data (Hoeffken, 1987).

An MIR electron density computed with 3.0 Å data showed a reasonable solvent contrast and some secondary structure elements, but was too noisy

for extensive chain tracing. Therefore, two-fold averaging was carried out to improve the isomorphous phases.

A preliminary transformation matrix was obtained by the identification of a set of 2 × 4 heavy atom sites related by a local two-fold symmetry axis inclined at 8° to the crystallographic dyads.

A more precise transformation operator was determined by Patterson and real-space rotation and translation functions. To this end, a protein envelope was created from a solvent-flattened 4 Å MIR map using XCONTOUR (Buchberger, 1991). Since no boundaries between individual PTPS monomers were distinguishable in this electron density, the envelope was made around a PTPS hexamer, which comprises the content of half of the unit cell. The MIR map inside the envelope was transferred into an artificial P1 cell with cell axes increased by a factor of 1.5. Back transformation of this map yielded structure factors that were used for the calculation of a Patterson function. A self-rotation function computed from this Patterson retained the crystallographic peak at polar angles (90°, 90°, 120°) due to the presence of two crystallographic trimers in the masked map, but lacked the signal of the crystallographic dyads. Instead, the peaks of the local symmetry operation appeared at polar angles (37.6°, 0.0°, 180°) with a peak height of 0.7 relative to the crystallographic peak. Subsequently, the orientation and location of the local axis were refined by alternate rotation and translation direct space correlation functions in PROTEIN.

Two-fold averaging was performed with the program MAIN (Turk, 1992) within the above determined hexamer envelope. Twenty cycles of averaging and combination of the phases obtained by back transforming the averaged maps and the MIR phases at 3.0 Å resolution (back transformation *R*-factor: R_S = 38.5%, R_E = 22.9%, <FOM> = 0.81) produced a map with greatly improved features which was readily interpretable in most regions. However, around the mercury-binding site of the HGAC derivative, the electron density was dominated by a large cluster of peaks and was not interpretable before MIR phases had been replaced by model phases in the final steps of model building and refinement.

A partial model including 82 polyalanine residues in six polypeptide segments was built and refined with XPLOR. Model phases were combined with MIR phases and the molecular averaging procedure iterated. After three rounds of model building and refinement, residues 7–144 (rat DNA sequence) had been placed in the density and the *R*-factor had decreased to 26.0% (data from 8.0 to 2.3 Å).

The current model comprises 2204 protein atoms, two metal ions and 85 solvent atoms, all of which are very well defined in a $2F_o-F_c$ electron density contoured at 1.2σ. The crystallographic *R*-factor is 20.4% for 21 405 reflections from 8.0 to 2.3 Å resolution. The r.m.s. deviations from ideal stereochemistry are 0.010 Å for bond length and 1.61° for bond angles [force field parameters from Engh and Huber (1991)]. The dihedral angles of the polypeptide backbone all lie in allowed regions of the Ramachandran diagram. The two independent monomers are related by a local dyad axis with polar angles (37.5°, 0.2°, 180.0°) which cuts the crystallographic triad at (2/3, 1/3, 27.8 Å). They have a r.m.s. difference of main chain atomic positions of 0.16 Å.

Acknowledgements

The financial help from the Helmut Horten Research Foundation and the Swiss National Foundation (grant no. 31-33897.92) is gratefully acknowledged.

References

Blau,N. (1988) *Annu. Rev. Nutr.*, **8**, 185–209.
Blau,N., Thöny,B., Heizmann,C.W. and Dhondt,J.-L. (1993) *Pteridines*, **4**, 1–10.
Brünger,A. (1988) *J. Mol. Biol.*, **103**, 803–816.
Buchberger,M. (1991) Diploma Thesis, Technische Universität München, München.
Bürgisser,D.M., Thöny,B., Redweik,U., Hunziker,P., Heizmann,C.W. and Blau,N. (1994) *Eur. J. Biochem.*, **219**, 497–502.
Curtius,H.-C., Heintel,D., Ghisla,S., Kuster,T., Leimbacher,W. and Niederwieser,A. (1985) *Eur. J. Biochem.*, **148**, 413–419.
da Silva,J.J.R.F. and Williams,R.J.P. (1991) In *The Biological Chemistry of the Elements*. Clarendon Press, Oxford.
Doi,K., Antanaitis,B.C. and Arsen,P. (1988) *Struct. Bonding*, **70**, 1–26.
Engh,R.A. and Huber,R. (1991) *Acta Crystallogr. Sect. A*, **47**, 392–400.
Guzman,J., Redweik,U., Schoedon,G., Hunziker,P., Wiestler,O.D., Heizmann,C.W. and Blau,N. (1992) *Enzyme*, **46**, 287–298.
Hasler,T. and Curtius,H.-C. (1989) *Eur. J. Biochem.*, **180**, 205–211.
Hauer,C.R., Leimbacher,W., Hunziker,P., Neuheiser,F., Blau,N. and Heizmann, C.W. (1992) *Biochem. Biophys. Res. Commun.*, **182**, 953–959.
Hoeffken,W. (1987) PhD Thesis, Technische Universität München, München.
Inoue,Y., Kawasaki,Y., Harada,T., Hatekayama,K. and Kagamiyama,H. (1991) *J. Biol. Chem.*, **266**, 20791–20796.
Jones,T.A. (1978) *J. Appl. Crystallogr.*, **15**, 24–31.
Kaufman,S., Berlow,S., Summer,G.K., Milstien,S., Schukman,J.D., Orloff,S., Spielberg,S. and Pueschel,S. (1978) *N. Engl. J. Med.*, **299**, 673–679.
Kaufman,S., Pollock,R.J., Summo,G.K., Das,A.K. and Hajra,A.K. (1990) *Biochim. Biophys. Acta*, **1040**, 19–27.
Kerler,F., Schwarzkopf,B., Katzenmeier,G., Le Van,Q., Schmid,C. and Bacher,A. (1989) *Biochim. Biophys. Acta*, **990**, 15–17.
Kwon,N.S., Nathan,C.F. and Stuehr,D.J. (1989) *J. Biol. Chem.*, **264**, 20496–20501.
Le Van,Q., Katzenmeier,G., Schwarzkopf,B., Schmid,C. and Bacher,A. (1988) *Biochem. Biophys. Res. Commun.*, **151**, 512–517.
Levitt,M. and Chothia,C. (1976) *Nature*, **261**, 552–558.
Masada,M. (1993) In Ayling,J.E., Nair,M.G. and Baugh,G.M. (eds), *Chemistry and Biology of Pteridines and Folates*. Plenum Press, New York, pp. 191–194.
Milstien,S. and Kaufman,S. (1985) *Biochem. Biophys. Res. Commun.*, **128**, 1099–1107.
Nichol,C.A., Smith,G.K. and Duch,D.S. (1985) *Annu. Rev. Biochem.*, **54**, 729–764.
Niederwieser,A., Blau,N., Wang,M., Joller,P., Ataris,M. and Cardesa-Garcia,J. (1984) *Eur. J. Pediatr.*, **141**, 208–214.
Orengo,C.A. and Thornton,J.M. (1993) *Structure*, **1**, 205–216.
Parge,H.E., Arvai,A.S., Murtari,D.J., Reed,S.I. and Tainer,J.A. (1993) *Science*, **262**, 387–395.
Park,Y.S., Kim,J.-K., Jacobsen,K.B. and Yim,J.J. (1990) *Biochim. Biophys. Acta*, **1038**, 186–194.
Schmid,C., Meining,W., Weinkauf,S., Bachmann,L., Ritz,H., Eberhardt,S., Gimbel,W., Werner,T., Lahm,H.-W., Nar,H. and Bacher,A. (1993) In Ayling,J.E., Nair,M.G. and Baugh,G.M. (eds), *Chemistry and Biology of Pteridines and Folates*. Plenum Press, New York, pp. 157–162.
Scriver,C.R., Kaufman,S. and Woo,S.L.C. (1989) In Scriver,C.R., Beaudet,A.L., Sly,W.S. and Valle,D. (eds), *The Metabolic Basis of Inherited Disease*. McGraw-Hill, New York, Vol. 1, pp. 95–546.
Smith,G.K. and Nichol,C.A. (1983) *Arch. Biochem. Biophys.*, **227**, 272–278.
Steigemann,W. (1974) PhD Thesis, Technische Universität München, München.
Takikawa,S.I., Curtius,H.-C., Redweik,U., Leimbacher,W. and Ghisla,S. (1986) *Eur. J. Biochem.*, **161**, 295–302.
Tayeh,M.A. and Marletta,M.A. (1989) *J. Biol. Chem.*, **264**, 19654–19658.
Turk,D. (1992) PhD Thesis, Technische Universität München, München.
Thöny,B., Leimbacher,W., Bürgisser,D. and Heizmann,C.W. (1992) *Biochem. Biophys. Res. Commun.*, **189**, 1437–1443.
Thöny,B., Leimbacher,W., Blau,N., Harvie,A. and Heizmann,C.W. (1994) *Am. J. Hum. Genet.*, in press.
Turk,D. (1992) PhD Thesis, Technische Universität Münchenm München.
Weiss,M.S., Abele,U., Weckesser,J., Welte,W., Schiltz,E. and Schulz,G.E. (1991) *Science*, **254**, 1627–1630.

Received on December 3, 1993; revised on December 23, 1993